T.1: Copper-HBr laser activity at RRCAT: Development and Studies

Ramakanta Biswal
Metal Vapour & Dye Laser Application Laboratory
Laser Systems Engineering Section
E-mail: rbiswal@rrcat.gov.in

1. Introduction

Copper-HBr laser (Cu-HBrL), also known as Copper-HyBrID laser, that produces coherent radiations at green (510.6 nm) and yellow (578.2 nm) wavelengths, is a lower temperature (~550 °C) and highly performing variant of atomic copper laser in important aspects such as specific average output power, pulse repetition rate (PRR), beam quality and efficiency [1-3]. Often this laser is an alternative to frequency doubled solid-state lasers with some advantages for applications that require high PRR (~ 5-25 kHz), high spectral brightness as well as stability in the visible and its frequency doubled ultraviolet (UV) region. These features of a Cu-HBrL enhances the scope of applicability of the copper laser such as in high PRR pumping of tunable dye & Ti:sapphire lasers, high PRR UV generation and high speed precision material processing etc.

Conventional copper vapour laser (CVL) operates at temperature of ~1500 °C and PRR of 5-6 kHz with ~1% efficiency. This high temperature operation requires the laser start-up/cool-down time of around one hour and poses difficulties on laser engineering as well as obtaining high beam quality laser output. In contrast, Cu-HBrL is a lower operating temperature (~550°C) device with fast start-up/cool-down time (10-15 minutes) and produces higher (2 to 3 times) average output power at 15-20 kHz PRR with much better laser beam quality and ~2% efficiency. Due to lower working temperature, a Cu-HBrL is compact, light weight and can be made air cooled even at high average power (~100 W) in contrast to the conventional CVLs [4,5].

In view of the above perspective, a program was taken up to develop the Cu-HBrLs in Laser System Engineering Section of RRCAT. The Cu-HBrL technology was successfully developed culminating to several versions upto average laser power of 110 W (Fig.T.1.1, Table. T.1.1). The present article briefly describes the technology development activities and related studies carried out on various aspects of the Cu-HBrLs. At the end, some initial results on the development of 15-20 kHz PRR tuneable dye laser as well as coherent UV source through frequency doubling by using this pump laser are presented.

Fig.T.1.1: Photograph of 100 W average power class (max.: 110 W), 18 kHz PRR Copper-HBr laser developed in RRCAT

2. Physics of Copper-HBr laser

The basic physics associated with lasing process of a Cu-HBrL is similar to that of the CVL. In both the cases the lasing transitions are obtained in copper atom. However, the method of production of the lasant copper atoms in the laser discharge and some associated laser kinetic processes are different in a Cu-HBrL, which enable it to be highly performing. In a Cu-HBrL, gas mixture of HBr and neon (Ne) (6-7% HBr + balance Ne) gas is injected into the discharge region. The injected HBr gas and its dissociation products in the discharge (i.e., Br/H) react chemically with copper pieces placed along the floor of the discharge tube to produce copper bromide (CuBr) vapors at temperature of ~550 °C (i.e., Cu + HBr → CuBr/CuH +H/Br & Cu+Br/H→CuBr/CuH). These molecules of CuBr then polymerize to Cu_xBr_x (x=3,4) and diffuse into the discharge region. The electron-impact dissociation of these copper precursors leads to release free copper atoms [6,7]. These undergo excitation in the same pulse to produce population inversion between its resonance ($^2P_{3/2,1/2}$) and meta-stable ($^2D_{3/2,5/2}$) levels for lasing action as in CVL. The population inversion exists only for <100 ns.

During inter-pulse period, the metastable levels decay to ground level via super-elastic collisions with Ne, Cu and electrons as well as by energy transfer collision with H_2 present as dissociation product of HBr. The lower operating temperature as well as availability of additional channel for metastable level relaxation by H_2 helps in improving the laser performance as compared to the CVL. The HBr improves the laser level kinetics through its resonant dissociative attachment (DA) of inter-pulse electrons followed by mutual ion-ion neutralization ($HBr + e^- \rightarrow H + Br^-$, $Cu^+ + Br^- \rightarrow Cu + Br$). This process proceeds rapidly during inter-pulse period with a rate constant of ~10^{-9} cm^3/sec, hence efficiently reducing the pre-pulse electron density and increasing recovery of ground state copper density. In a Cu-HBrL,

typical pre-pulse electron density (n_{eo}) attained is of ~0.1% of the peak value of ~10^{14}/cm^3 vs. that of ~30% for the CVL, whereas available pre-pulse ground state copper density is an order higher than that of the CVL (~10^{16}/cm^3 vs. ~10^{15}/cm^3). The lowering of pre-pulse electron-density leads to better radial & temporal homogenization of the applied electric field through reduced plasma skin effect. In addition, increased pre-pulse plasma impedance due to lowering of n_{eo} leads to better coupling of pump energy from the electrical pulser to the laser discharge and also enable it to hold higher voltage required for efficient pumping. These processes enable a Cu-HBrL to operate at higher PRR (~20 kHz vs. ~5 kHz) as well as higher efficiency (~2% vs. ~1%) than that of a CVL.

3. Indigenous development of Cu-HBr lasers

The development Cu-HBrLs relied on the successful development and integration of various subsystems. These needed to be compatible with HBr which is a highly reactive gas and degrades materials in presence of moisture. This involved suitable thermo-mechanical design of the laser electrodes & discharge tube, precision gas & vacuum handling system for HBr with over-all helium leak integrity ~ 10^{-8} mbar-lit./s or better. In addition, the development and integration of efficient high voltage pulser capable of operating at ~20 kHz with typical peak excitation voltage of about 20-25 kV and rise time of about 70-80 ns or less, was required. All the subsystems were indigenously designed and developed.

3.1 Laser head & discharge tube

Fig.T.1.2 shows the schematic of discharge tube and electrode assembly of Cu-HBrL. Two types of discharge tube, namely fused silica glass & alumina, have been used by us in Cu-HBrL [5,8]. However, fused silica glass has advantage of low cost, light weight, excellent thermo-mechanical properties and ease of fabrication. The fused silica discharge tube, designed and fabricated in-house, had its both ends flared. At the low voltage side, there was provision to inject HBr + Ne gas mixture just at the start of the discharge region (Fig. T.1.3). In other version, the alumina tube was sleeved within the fused silica envelope, where HBr + Ne gas mixture was injected into the discharge through a fused silica capillary tube [9]. Fused silica discharge tubes of 5-6 cm bore diameter and length 130-200 cm have been developed for different laser power versions. The tubes were either air cooled or sleeved within water cooled SS jacket (Fig. T.1.1, T.1.4). High purity cylindrical copper electrodes (~5 mm thick wall) having a small hole (~3 mm dia. x ~5 mm deep) drilled on the face of each, promoted stable discharge operation. These were press-fitted into water cooled stainless steel end flanges and were projected 5-10 cm into the discharge region and vacuum sealed at its both ends using Viton O-rings. A pair of fused silica disks attached to the electrode ends by Viton O-rings at ~5° inclination with respect to the laser tube axis, served as vacuum sealing end window. A corrosion resistant stainless steel diaphragm vacuum gauge (Leybold DIAVAC DV 1000) was used to monitor the pressure of HBr + Ne mixture. The whole assembly was tested for helium leak integrity better than 10^{-8} mbar-lit./s.

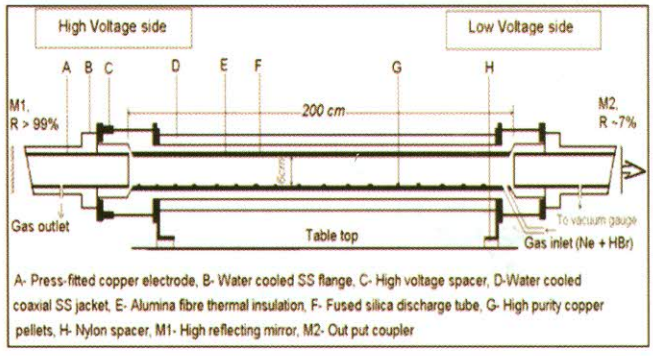

Fig.T.1.2: Schematic of the discharge tube & electrode assembly for Cu-HBrL

Fig.T.1.3: Fused silica discharge tube for Cu-HBrL

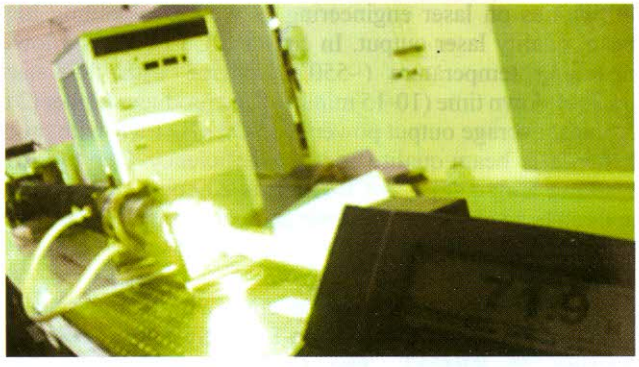

Fig.T.1.4: High specific output power (70 W/liter), 18 kHz PRR Cu-HBrL in operation at RRCAT

All the wetted parts were of either high purity copper or fused silica which ensured minimum level of impurity in the discharge. Depending on the input power level used, a thin (1-3 mm) layer of alumina fibre insulation was wrapped on the fused silica discharge tube to ensure desired temperature. However, in other model where the alumina tube was used as discharge tube, no thermal insulation was required to

attain/maintain the desired operating temperature (Fig. T.1.4). Several high purity copper pieces (15 x 10 x 3 mm^3), which were machined for smoothness, were placed inside the discharge tube along its floor at regular intervals of ~10 cm.

3.2 Gas and vacuum handling system for HBr

The key issues associated with development of Cu-HBrL are the reliable control and safe handling of HBr concentration to protect the components from failure. For this, a microprocessor based precision gas mixing set up, consisting of thermal mass flow controller (for Ne) and ultra-precision compatible needle-valve/mass flow controller (for HBr), was designed & fabricated (Fig. T.1.5). This unit was tested for helium leak integrity of better than 10^{-8} mbar. lit./s. It controlled the HBr mass flow rate from 1 to 99 cc/min., with accuracy of 0.5 cc/min., and HBr concentration from 0.5 to 10% with accuracy of 0.5%. Similarly, a stainless steel vessel containing activated charcoal, silica gel & pellets of calcium hydroxide/ carbonate was used in between the exhaust end of the laser tube and vacuum pump. This ensured neutralization of HBr after coming out from the Cu-HBrL tube and before its release as exhaust.

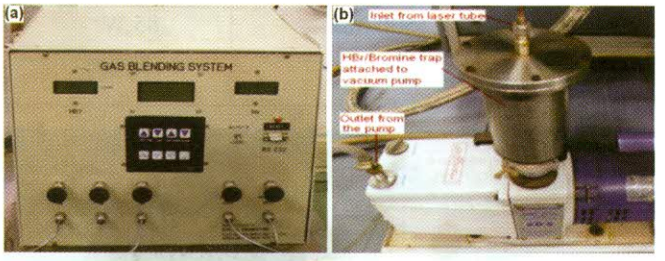

Fig.T.1.5: HBr gas handling system developed (a) HBr & Ne mixing set up, (b)HBr/Bromine trap

3.3 High voltage electrical pulse power supply

The electrical pumping pulse power technology plays a very crucial role in deciding the Cu-HBrL performance. Electrical energy from regulated DC source was fed to storage capacitor through LC-resonant charging. The stored high voltage was switched at desired multi-kHz PRR with fast pulse rise time (<100 ns). The high voltage (~10's of kV), high PRR (~20 kHz), fast switching was achieved in two schemes - by using a thyratron switch based pulse modulator or using IGBT switch modulator consisting of 4 IGBTs in parallel, pulse step up transformer & 3 stages of magnetic pulse compressors (MPCs). The later version of the modulator could be operated at average switched electrical power of 5-10 kW at PRR of 16-18 kHz, peak tube voltage of 20-25 kV with rise time of 70-80 ns. The thyratron based modulator could be operated upto 4-4.5 kW with PRR 15-20 kHz [10]. While the thyratron based system was employed in low power version of Cu-HBrL (40 W laser output power @ 18 kHz PRR), the higher output power version lasers were based on IGBT solid state pulsers (Fig. T.1.6) [11]. The solid state pulser was used to maximum IGBT switching voltage of 800 V, for safety reason, and was stepped up by the pulse transformer of turn ratio ~1:32 followed by 3 stage pulse compression in MPCs with net gain of ~23.

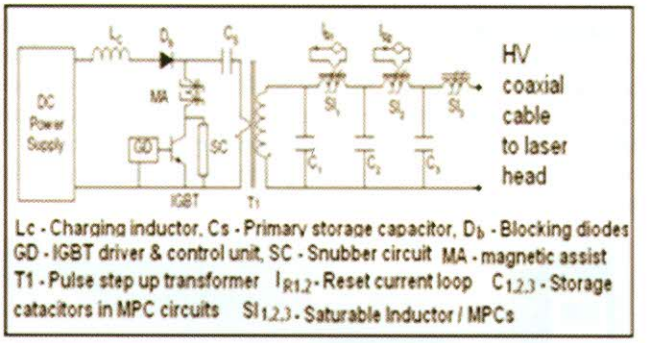

(a)

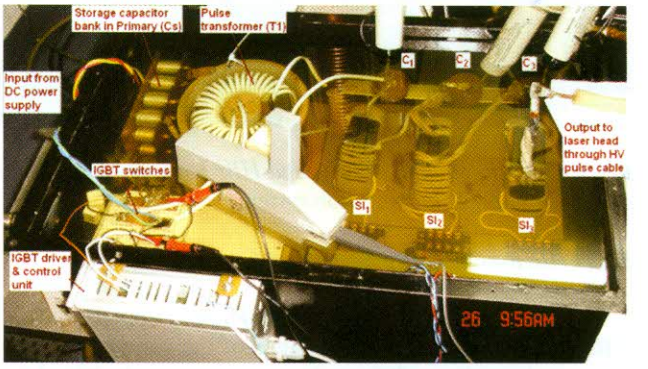

(b)

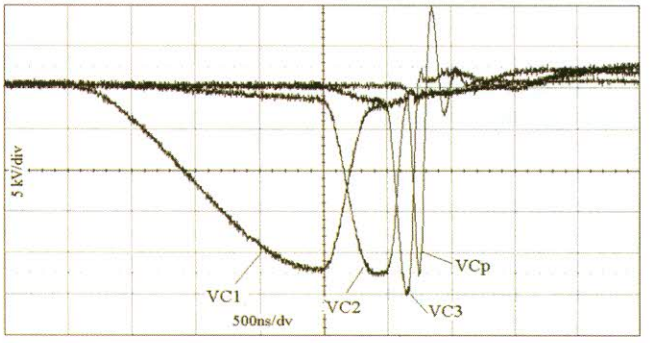

(c)

Fig.T.1.6: (a) Schematic (b) Photograph and (c) pulse compression waveforms of the developed IGBT switch based solid state pulser for Cu-HBrL

3.4 Safety systems for HBr handling

In the presence of moisture, HBr (TLV=3 ppm) corrodes/degrades most of the metals. Therefore all the wetted parts involved were made of SS-316 with ensured helium leak integrity of the joints/assemblies better than 10^{-8} mbar-lit./s. In addition, all the components are periodically purged with dry inert gases (N_2/Ar) and checked for vacuum/pressure withstanding integrity. The laboratory is made adequately ventilated and is continuously monitored for accidental HBr leakage as well as for the ambient oxygen level. For this, suitable sensor and control & alarm systems (Fig.T.1.7), were installed in the laboratory. The laboratory is also equipped with personal protective equipments for handling of accidental HBr leakage.

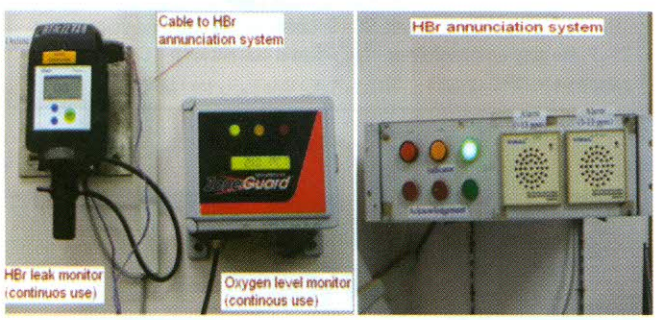

Fig.T.1.7: Photograph of installed HBr leak sensor, ambient oxyegn monitor & anunciation system.

3.5 Performance of the developed Cu-HBrLs

Fig.T.1.8 shows the variation of laser output power with different storage capacitor voltages of the solid state pulser for 6 cm bore dia. x 200 cm long discharge tube based Cu-HBrL (Fig. T.1.1). The maximum laser output power achieved was 110 W at storage capacitor voltage of 800 V. It clearly indicates still higher laser power can be obtained with increase of the voltage/input power. Table T.1.1 summarizes the various Cu-HBrLs developed, mainly differing in their discharge tube dimensions and producing average output power upto 110 W at PRR of 16-18 kHz (Fig. T.1.9). The 40 W version Cu-HBrL, which was pumped with thyratron based pulser, has been operated in the PRR regime of 15 to 27 kHz producing average output powers in the range of 25 to 40 W without degradation of beam quality. The 70 W version is a compact Cu-HBrL pumped by solid state modulator and produced specific output power ~70W/liter at 18 kHz PRR with excellent beam characteristics (Fig. T.1.4). Most of the spatial and spectral characteristics studies were carried out using this laser.

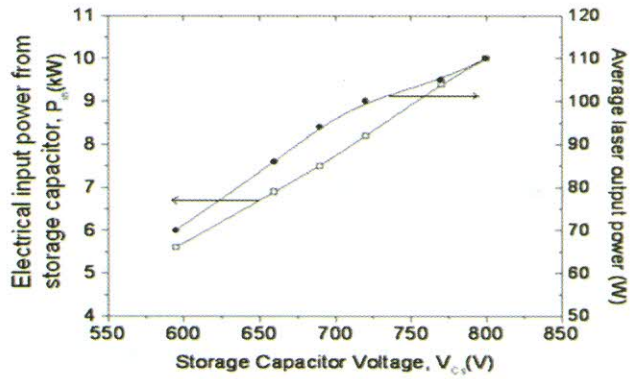

Fig.T.1.8: Variation of laser output power & switched input power with storage capacitor voltage

Table T.1.1: Summary of various Cu-HBrLs developed

Sl. No.	Laser tube dimension (ID x Length)	Average laser output power
1	50 mm x 1300 mm	40 W
2	47 mm x 1500 mm	70 W
3	58 mm x 1500 mm	85 W
4	60 mm x 2000 mm	110 W

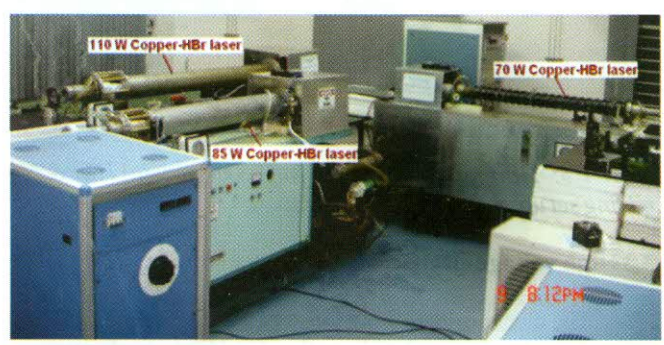

Fig.T.1.9: The Cu-HBrLs developed in LSES, RRCAT

4. Pulse pumping behaviour of Cu-HBr laser

The Cu-HBrL employs fast high voltage electrical pulse at 15-20 kHz PRR for lasing action. The electrical pumping efficiency is governed by the fraction of input pulse energy coupled to the laser plasma, specifically within first 100 ns from onset of the pulse. The HBr additive affects the discharge characteristics of the Cu-HBrL by the way of controlling the evolution and distribution of electron/ion density. Hence, to understand and optimize the performance of Cu-HBrLs, the pulse pumping characteristics such as the temporal pattern of the electrical power deposition were

studied by numerical processing of the laser head voltage-current waveforms (Fig. T.1.9)[12].

The Cu-HBrL as an electrical circuit element can be approximated as a series combination of laser tube/circuit-loop inductance (L) and gas discharge resistance (R).Therefore, the instantaneous voltage measured across the laser tube i.e., $V(t)$, is the sum of the voltage across L. For a given operating condition and geometry, the laser tube inductance L is constant. This is determined from the laser head voltage-current waveforms at the first zero of the current waveform at $t = t_0$ i.e., $L = [V(t)_{t=to}/[(dI/dt)]_{t=to}$ (Fig. T.1.10). The instantaneous and average values of the electrical power dumped to the Cu-HBrL plasma were, $P_{dump}(t) = [V(t) - L.dI(t)/dt]\ I(t)$ and $P_{dump} = PRR\ [\int_0^T [V(t) - L.dI(t)/dt].I(t)/dt]$, where $I(t)$ & T are the instantaneous discharge current & inter-pulse period respectively. By varying the limit of integration, power deposition pattern in the desired time interval was carried out.

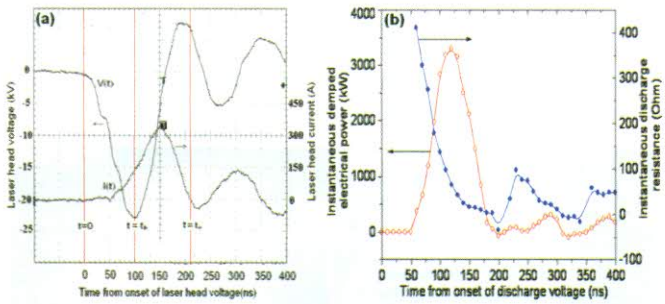

Fig.T.1.10: Typical (a) laser head voltage-current waveforms and (b) Instantaneous electrical power dumped & resistance in Cu-HBrL at 110 W power.

4.1 Role of laser operating parameters

Both time resolved & time averaged analysis of the pumping characteristics of the Cu-HBrLs was carried out by numerical processing of measured laser head voltage-current waveforms for various operating parameters such as input switching voltage, HBr concentration, buffer gas flow rate, buffer gas pressure and pulse repetition rate. Process controlling discharge plasma parameters such as the electrical inductance, electrical resistance, active laser head voltage, active electrical power, pre-pulse electron density and axial gas temperature were evaluated and a correlation was established with the Cu-HBrL performance. At 110 W laser output power, the switched input power was 10 kW, out of which around 40% of the electrical input power was coupled into the Cu-HBrL plasma to provide lasing action. The rest 60% was dissipated mostly in the MPCs of modulator. Similarly, the HBr concentration and buffer gas flow rate had dominant effects on the behaviour of electrical energy coupling and hence on the laser output power. The buffer gas pressure and pulse repetition rate of scanned ranges had similar but relatively less effect on the energy coupling behaviour. In a separate study on comparison of discharge characteristics of a Cu-HBrL and conventional CVL, it was observed that the Cu-HBrL plasma favours faster energy deposition leading to its better performance as compared to the CVL and the reason was attributed to the improved pre-pulse impedance of the plasma [12].

4.2 Role of HBr purity

Due to extremely corrosive and moisture sensitive nature of the HBr, its dissociation and reactant products affect the available gas purity. Any impurity present in HBr gas also affects the evolution of the electron energy distribution and degrades the performance of a Cu-HBrL. So, the HBr gas used should be free from its dissociation products i.e., free hydrogen and bromine. In view of this, a set up was developed to purify the HBr gas through two stage fractional distillation technique (i.e., H_2 & Br_2 were trapped at -196 °C & -20 °C respectively) and assessed by mass spectrometric analysis before and after distillation (Fig. T.1.11). The effect of such purified HBr gas on the Cu-HBrL discharge and output performance characteristics (average output power, efficiency and beam diameter) were studied [13].

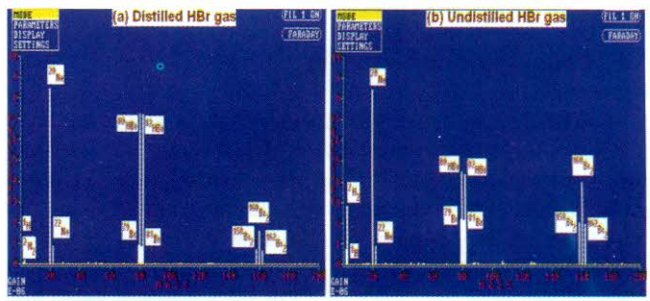

Fig.T.1.11: Mass spectra of (a) Distilled HBr gas and (b) Undistilled HBr gas

Around 37% improvement in the average laser output power (from 40 to 55 W) was observed by use of this distilled HBr gas as compared to the undistilled one, at otherwise same laser operating condition. The improvement in the Cu-HBrL performance with distilled HBr gas was attributed to lowering of free H_2 and Br_2 concentration, which otherwise acted as poison for Cu-HBrL. The lowering of the impurities enhanced the DA process for reduction of n_{eo}, higher pre-pulse plamsa impedance (~2.5 kΩ vs. ~1.2 kΩ) and hence improved the energy coupling from the pulser to the laser plasma (Fig. T.1.12). This was mainly manifested as the increased average electrical power dumped to the discharge within first 100 ns

(from 2.6 to 3.0 kW) at faster rate thereby larger laser gain as well as increased gain volume due to increased radial extent of electric discharge because of increase in laser beam diameter (from 30 mm to 40 mm).

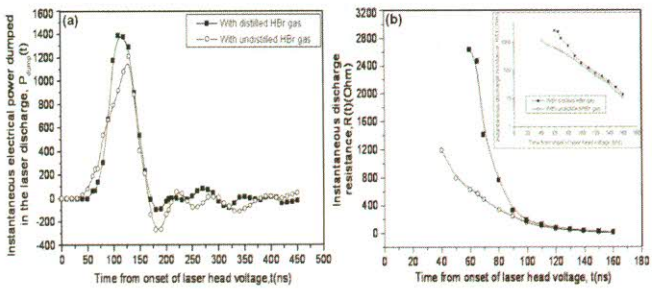

Fig.T.1.12: Temporal pattern of (a) energy deposition and (b) discharge resistance for distilled and undistilled HBr gas

5. Spatial & spectral behaviour of Cu-HBr laser

Knowledge of spatial and spectral characteristics of a Cu-HBrL is very important not only for understanding the laser kinetics but also for planning for its applications. With this view, a comprehensive study was carried out on spatial (thermal lensing, spatial & temporal intensity profiles, far-field beam divergence & pointing stability etc.) and spectral (emission line-width & its stability) of both the green (G) and yellow (Y) radiation of the Cu-HBrL.

5.1 Thermal lensing behaviour

The thermal lensing behaviour of a Cu-HBrL is due to non-uniform radial temperature distribution of the gain medium and the vacuum sealing glass windows used. It plays an important role in deciding the quality of the laser output beam. This aspect of a Cu-HBrL was studied by shear interferometer technique and was compared with that of a CVL of identical geometry (4.7 cm ID x 150 cm long) and electrical excitation conditions operating at their optimum laser power condition (60 W @ 18 kHz for Cu-HBrL & 30 W @ 5.5 kHz for CVL). The results were analyzed in terms of radial temperature distribution and heat flux reaching at the laser glass windows and its absorption [14].

An expanded and collimated probe He-Ne laser beam, matching to the internal diameter of discharge tubes, was passed through the heated active medium and window. It was then incident on a shear plate at 45^0. The focal distance of net thermal lens, F_c, was estimated from the amount of rotation of fringes at observation plane as, $F_c = Sd/(\lambda \sin\theta)$, where S = the lateral shear distance = $(t \sin 2i) / (n^2 - \sin^2 i)$, d= the fringe spacing = $\lambda / 2n\alpha$), λ = He-Ne laser wavelength (632.8 nm), θ = rotation angle of the fringes, t = average thickness of the wedge plate (10 mm), i = angle of incidence (45^0), n = refractive index of the wedge plate material BK-7 glass (1.515 @ 633 nm) and α = angle of the wedge plate (20 arc-sec). The fringes were captured using a CCD camera with frame grabber card and the rotation angle of the fringes (θ) was estimated for both the cases (Fig. T.1.13). For measurement of window thermal lens, the expanded & collimated He-Ne laser beam was incident normal to the optical window of the laser. The heated optical window behaved as a lens which led the shear fringes to develop curvature (Fig. T.1. 14). The combined focal length of both the windows was, $F_w = (r_m^2 - r_n^2) / 2(m-n)\lambda$ where r_m and r_n are the radii of the m^{th} and n^{th} fringes respectively. It was observed that the net thermal lens power was dominated by lensing action due to fused silica windows because of their higher temperature coefficient of refractive index ($\sim +10^{-6}$/K) than that of the gaseous active medium ($\sim -10^{-10}$/K). The net thermal lens power of the Cu-HBrL was of around + 0.95 mD whereas that of the CVL was around +13 mD. The thermal lens power of due to the windows in the Cu-HBrL was too weak to be measured against around +15 mD for the CVL. The weaker thermal lens characteristics of the Cu-HBrL was attributed to its much lower working temperature and relatively flatter radial gas temperature profile (Fig. T.1.15).

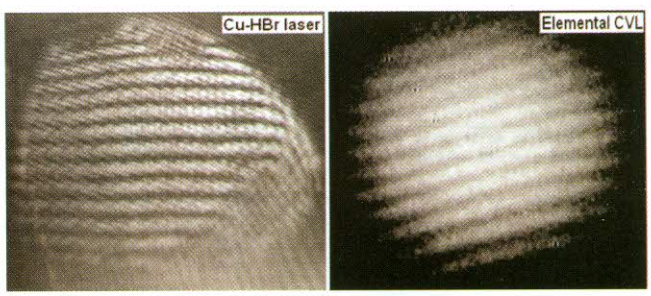

Fig.T.1. 13: Shear fringes of Cu-HBrL & CVL at their respective maximum laser power condition

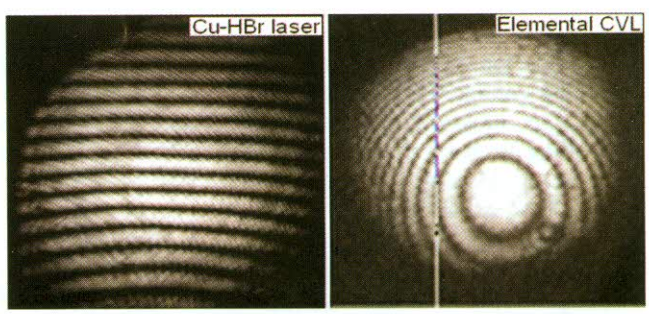

Fig.T.1.14: Shear fringes of heated laser windows of Cu-HBrL & CVL at maximum laser power condition

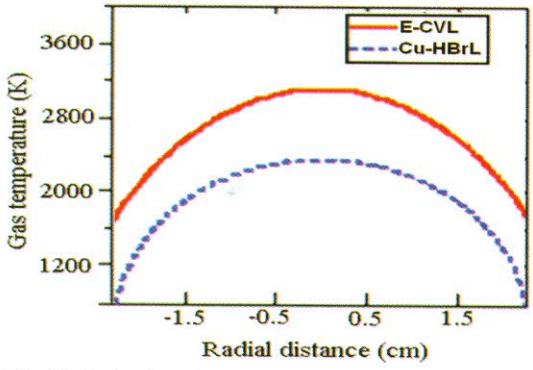

Fig.T.1.15: Calculated radial gas temperature profile for Cu-HBrL and CVL at max. laser power condition

5.2 Radial & temporal dynamics

Studies on radial and temporal dynamics were carried out for a 40 W version Cu-HBrL operating at 18 kHz PRR and 30 W version CVL operating at 6.5 kHz PRR, both were of same geometry & under identical operating conditions [15]. The radial beam intensity profiles of both the lasers are shown in Fig.T.1.16. The output beam width was same as the discharge tube diameter for the CVL and it was ~60% (3 cm) of the discharge tube diameter for the Cu-HBrL. The radial intensity profile had on axis minimum in case of the CVL as compared to on axis maximum (quasi-Gaussian profile) for the Cu-HBrL. The laser start up and subsequent power build up time in case of the Cu-HBrL was almost one third that of the CVL (Fig. T.1.16).

The temporal evolution of G and Y components are shown Fig.T.1.17 for the Cu-HBrL and the CVL. The evolution Y component in CVL was slow and much delayed with respect to the G as compared to that of the Cu-HBrL. However, in case of the Cu-HBrL, the pulse durations as well as the existence of gain maxima for both the radiation components were longer as compared to the CVL. The difference in characteristics of the Cu-HBrL from the CVL was mainly due to the presence of HBr and its dissociation products. These reduce the inter-pulse (low energy) electron density in the discharge primarily by resonant dissociative attachment process (i.e., $e+HBr \rightarrow H+Br^-$ or H^-+Br) and radiative attachment process (i.e., $e+Br \rightarrow Br^-+h\nu$ & $e+H \rightarrow H^-+h\nu$) [16]. The negative ions so formed by the above processes (i.e., Br^- & H^-) constrict the discharge by enhancing their recombination with copper ions (e.g., $Cu^++Br^- \rightarrow Cu+Br$ & $Cu^++H^- \rightarrow Cu+H$) which take place around the axial region because of higher degree of ionization of Cu on the axis (due to higher inter-pulse electron temperature as compared to the tube wall). Therefore, almost absence of the plasma skin effect (due to lowering of pre-pulse electron density by the DA processes) together with the discharge constriction, make the input electrical power to be concentrated around the axial region. Thus, the gain distribution peaks on its axis [12]. On the other hand, the absence of these effects and higher gas temperature in the CVL make the gain lower at the axial region as compared to wall, therefore the intensity distribution has central minimum.

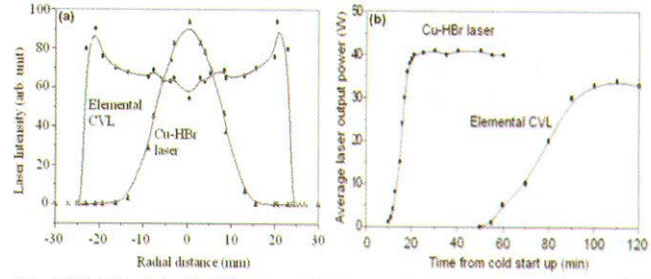

Fig.T.1.16: (a) Build up of laser output power & (b) Radial intensity profiles in the Cu-HBrL and the CVL

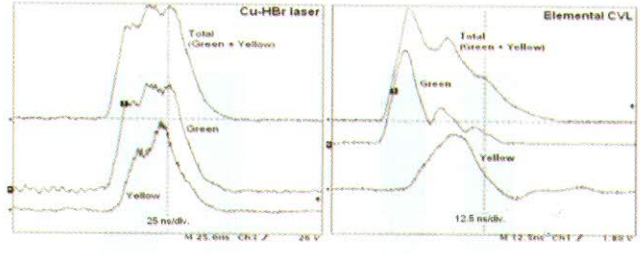

Fig.T.1.17: Temporal intensity profiles both G & Y radiations of the Cu-HBrL and the CVL

The earlier start up lasing action and faster build up of output power in the Cu-HBrL was due to its lower working temperature as well as better coupling of electrical energy from the pump source to laser the discharge because of lower n_{e0} ($\sim 10^{11}$ cm^{-3}) as compared to the CVL ($\sim 10^{13} cm^{-3}$). Longer gain duration as well as gain maxima in case of the Cu-HBrL was due to relatively less depletion of ground state copper atoms to meta-stable level due to its lower operating temperature.

5.3 Beam divergence & pointing stability

Comprehensive studies on the far-field beam divergence & pointing stability of both G and Y radiations of Cu-HBrL were carried out [17]. The spatial and energy characteristics i.e., pulse to pulse variation in average far-field divergence ($<\theta>$), pointing instability (δ) & intensity (I) vis-à-vis their fluctuations ($\Delta\theta$, $\Delta I/I$) of both the radiations were carried out with variation of switched electrical input power (6-9.5 kW) and HBr concentration (5-9%) for standard plane-plane resonator. The composite image (512 pulses spanning over 512 seconds) of the far-field spots were recorded and analyzed for estimation of the beam parameters (Fig.T.1.18, 19). The experimental observations were suitably supported by analysis in terms of input power coupling, thermally induced wave-front aberrations, contribution optical noise, laser kinetics, and effects of laser gain as well as its spatio-temporal distribution relevant to both the wavelengths.

The G/Y beams were focused by a lens L_1 (f_1= 50 cm) and filtered for ASE at the focal plane. This ASE filtered spot

was imaged with suitable magnification using another lens L_2 (f_2 = 25 cm) at the CCD head (Pixelfly qe, PCO AG of pixel size 6.45 μm x 6.45 μm). The images were captured by a PC & frame grabber card set up and were analyzed. The CCD acquiring time was set to 50 μs which was less than the inter-pulse time (~55.56 μs) that ensured single pulse recording. The individual line profiles stored in the allocated memory was saved as a composite/stacked image. These images were then analyzed for estimation of far-field beam characteristics. The error of measurement was limited by the pixel size of the CCD camera and was estimated as ± 5 μrad. The near-field spatial intensity profiles were recorded after suitably attenuating & imaging the laser exit on the CCD camera placed after the lens L_1. Part of the beam was also sampled to a fast biplaner photo-diode (Hamamatsu: R1193U-52) for monitoring the temporal pulse characteristics..

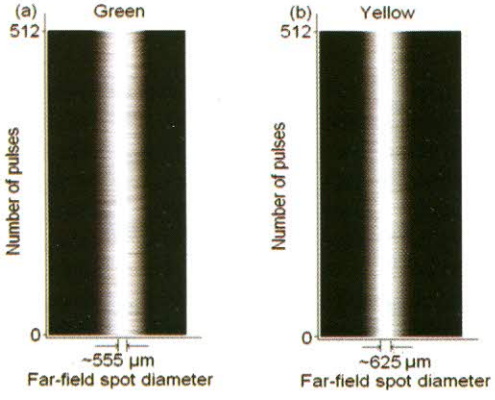

Fig.T.1.18: Typical composite pictures of the Cu-HBrL far-field spot for G and Y for 512 pulses

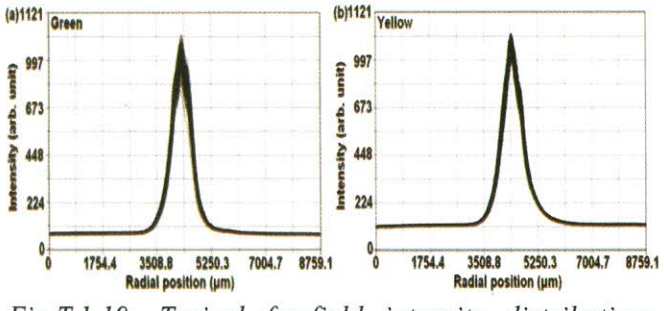

Fig.T.1.19: Typical far-field intensity distributions (composite) of the G and Y for the recorded 512 pulses

As the switched input power of the soild state pulser increased from 6 to 9.5 kW, <θ>,$\Delta\theta$, δ & ΔI/I increased monotonically from 1050 to 1090 μrad, ± 26 to ± 43 μrad, ± 27 to ± 50 μrad & ± 5.9 to ± 9.8% respectively for the G component and 1110 to 1300 μrad, ± 32 to ± 45 μrad, ± 25 to ± 53 μrad & ± 5.6 to ± 8.7% respectively for the Y component. Similarly, at fixed input power of 8 kW, for the HBr concentrations of 5% (below optimum), 7% (optimum) & 9% (above optimum) the values of <θ> were 1860 μrad, 1080 μrad & 1120 μrad for the G and 1883 μrad, 1215 μrad & 1392 μrad for the Y; the values of $\Delta\theta$ were ± 47 μrad, ± 33 μrad & ± 48 μrad for the G and ± 41 μrad, ± 38 μrad & ± 42 μrad for the Y; the values of δ were almost constant at ± 37-38 μrad for the G and ± 118 μrad, ± 37 μrad & ± 125 μrad for the Y; the values of $\Delta I/I$ were ± 11.5%, ± 7.2% & ± 9.0% for the G and ± 14.5 %, ± 6.4% & ± 8.7% for Y respectively. These results were compared with that of CVL published earlier [18]. The beam parameter values were <θ> = 3000 μrad, δ = ± 120 μrad and $\Delta I/I$ = ± 25% for the G component of the CVL. However, with unstable resonator of magnification 100, these values were <θ> = 122 μrad, $\Delta\theta$ = ± 15 μrad, δ = ± 15 μrad & $\Delta I/I$ = ± 30% for the green and <θ> = 108 μrad, $\Delta\theta$ = ± 10 μrad, δ = ± 10 μrad & $\Delta I/I$ = ± 45% for the Y component. This established the better spatial and energy characteristics of a Cu-HBrL over the CVL.

5.4. Spectral characteristics

The spectral emission characteristics of G & Y were studied both experimentally and theoretically [19]. A high resolution wavelength meter (Angstorm WS 7) was used to study the emission characteristics of the G/Y radiations and typical wave meter traces obtained are shown in Fig.T.1.20. The experiment was carried out with variation of switched electrical input power (6-9.5 kW) of the solid state pulser, HBr concentration (5-9%) and optical resonator (plane-plane & unstable) . These results were supported by comprehensive analysis line shape calculations taking into account the isotopic shift, hyperfine splitting, line broadening and temperature & gain distribution effects relevant to the Cu-HBrL. It was observed that in a Cu-HBrL, the line-width was affected by the electrical input power and HBr concentration whereas it is least affected by the optical resonators (plane-plane or unstable). The G component of the laser had lower spectral emission line-width and fluctuation as compared to that of the Y component. For 72 W output power Cu-HBrL, variation of electrical input powerfrom 6 to 9.5 kW (the laser power of the G & Y component increased from 23 to 38 W and 15 to 34 W respectively), the line-widths of the G & Y increased from 4 to 4.7 GHz and 6.5 to 9.3 GHz respectively. The corresponding line-width fluctuation also increased from 50 to 180 MHz and 60 to 575 MHz respectively for the G & Y. These line-width values were lower than those of the CVL of ~7 GHz & ~11 GHz respectively for the G & Y respectively.

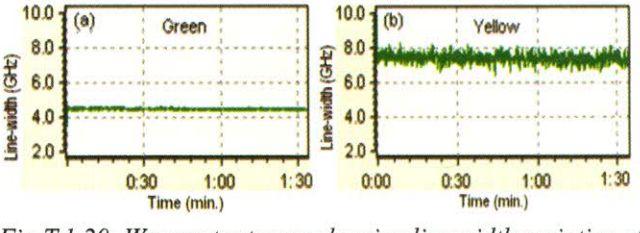

Fig.T.1.20: Wavemeter traces showing line width variation of the G & Y components of the Cu-HBrL

It was estimated that in standard operating conditions of a Cu-HBrL, the combined contribution of the natural broadening, resonance/self-broadening (due to Cu) and foreign gas broadening (due to H/H_2, Br/Br_2, HBr, Ne etc.) were significantly (10^2-10^3 times) lower than that of Doppler broadening. Therefore, Doppler broadening of each hyperfine component proceeds independently centered at different frequencies and their convolution produce the net line shape observed (Fig. T.1.21). Based on this analysis, a mathematical expression was formulated for estimation of line shape of each of the hyperfine transition vis-à-vis their convolution. The line shapes as well as their convolution for both the G & Y components were computed for different gas temperatures. The computed results explained the observed results. It was calculated that the G/Y line of Cu-HBrL consisted of total 18/12 hyperfine transitions of varying intensity and frequency shifts. The net estimated spread of the transition frequency shifts, taking into account all the hyperfine transitions, were ~8.63 GHz and ~12.64 GHz for the G and Y line respectively. The G line was dominated by a strong hyperfine component followed by three relatively weak components of intensity ratio 1.00: 0.62:0.45:0.35 and respective frequency shifts (with respect to central emission frequency) of -2.424 GHz, 0.165 GHz, -0.343 GHz & 1.909 GHz. Similarly, the Y line was dominated by a strong hyperfine component followed by four relatively weak components of intensity ratio 1.00:0.45:0.36:0.36:0.36 and respective frequency shifts of -3.819, -1.868 GHz, 0.858 GHz, 1.872 GHz & 4.422 GHz.

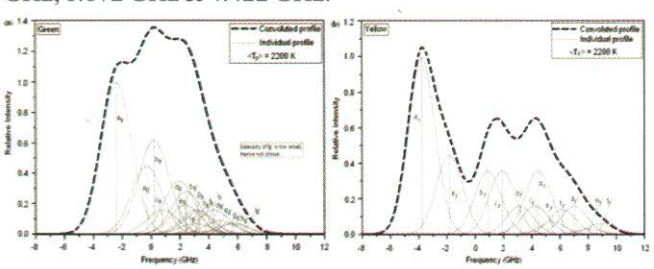

Fig.T.1.21 Typical calcultaed Cu-HBrL line-shape for (a) green line and (b) yellow line

6. Application of the Cu-HBr laser : Dye laser pumping & second harmonic UV generation

The developed Cu-HBrLs were used in two major applications in this group such as development of narrow line-width pulsed dye laser in orange-red wavelength (570-600 nm) region and generation of coherent UV (255.3 nm) radiation through nonlinear frequency doubling. For the development of 15-20 kHz PRR dye laser, required liquid dye (~ 1mM Rhodamine-6G in ethanol) flow system upto 12 lpm and a flat glass dye cell of size 15 mm x 10 mm x 0.7 mm (gap) have been developed in house. The dye laser, pumped by the green component of the Cu-HBrL at 18 kHz PRR with average power of 8 W, was characterized for output power and line-width behavior for different dye solution flow rates from 2 to 12 lpm [20]. The dye laser was operated in narrow band configuration with grazing incidence grating (2400 lines/mm) cavity and intra-cavity prism beam expander (M ~22) with overall cavity length of about 16 cm. Minimum dye laser line-width of ~2.2 GHz was obtained at the flow rate of 3-4 lpm where as the maximum dye laser power of ~620 mW was obtained at the flow rate of 9-10 lpm. The fluctuation in the line-width and wavelength of the dye laser at this 3-4 lpm flow rate were also minimum of ~400 MHz and ~0.003 nm respectively (Fig.T.1.22).

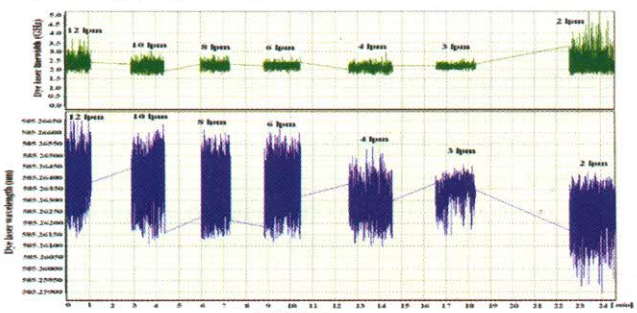

Fig.T.1.22: Line-width and wavelength of Cu-HBrL pump dye laser with different dye solution flow rates

The developed high beam quality, 15-20 kHz PRR Cu-HBrL is also being used for generation of coherent UV source (Fig.T.1.23). A BBO crystal (size: 6 x 8 x 7 mm^3, cut angle $\theta=51^0$, $\Phi=0^0$ for SHG of $\lambda=510.6$ nm for type-I phase matching), mounted on a five axis micro-position controller, was used as second harmonic converter. Diffraction limited green beam obtained from the 18 kHz PRR Cu-HBrL fitted with unstable resonator of magnification 15, producing pulse averaged beam divergence of ~260 μrad (~5 x DL) was used as the pump beam. This beam of 30 mm diameter was compressed to 3 mm to match well with the crystal dimension

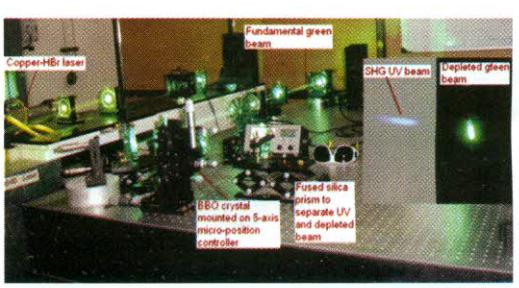

Fig.T.1.23: Photograph of the set up for 18 kHz PRR second harmonic UV generation of Cu-HBrL

and was then line focused using a cylindrical lens of focal length 4 cm. An average SHG UV (255.3 nm) power of ~ 700 mW at the pump power of 9.2 W and 18 kHz PRR, was obtained, corresponding to the average conversion efficiency of 7.5% and maximum instantaneous conversion efficiency of 15%. Further detailed study on optimization for efficient UV SHG process is in progress. This study and development may augment as a higher PRR UV source for ongoing CVL SHG UV based FBG writing activity.

7. Conclusions

The current article presented an overview of the research and development activities carried-out on most highly performing variant copper laser which is based on HBr additive (i.e. Cu-HBrL) vis-à-vis its ongoing applications. The activities involved indigenous design & development of the laser electrodes, discharge tube, gas handling system, suitable high power & high PRR pulse power supplies which culminated to successful development of several high average power Cu-HBrLs producing power as high as 110 W at 15-20 kHz PRR from a single system. The development activity was further augmented with many studies including evaluation of efficient pulse pumping mechanisms and detailed characterization of spatial & spectral beam qualities of both the green and yellow components of the Cu-HBrL. Following the successful developments and comprehensive characterization, these lasers are being used as pump sources for carrying out development and studies on 15-20 kHz PRR coherent UV source and tuneable dye laser. However, successful and long-term deployment of this laser is largely dependent on the resolution of the issues like handling of HBr, growth of copper (called dendrite) on the solid copper pieces in the laser tube and the laser window contamination due to deposition of copper compounds by diffusion.

Acknowledgements

The works presented in this article is an outcome of team effort in this section and is also a part of the author's on going Ph.D. dissertation. The author wishes to extend his sincere and deep gratitude to the thesis supervisor Dr. S. K. Dixit, Head, MVDLAL for his invaluable guidance & support and to Sh. S. V. Nakhe, Head, LSES for his constant support & encouragement for this work. The contribution of Sh. P. K. Agrawal for development of high voltage pulse power supplies for the Cu-HBrLs is highly acknowledged. Helpful discussions with Dr. Om Prakash are acknowledged. Supports from Sh. G. K. Mishra, Sh. S. K. Agrawal & other group members during the experiments and from glass blowing facility for fabrication of the fused silica laser discharge tube, are also acknowledged. Thanks are due to ex. Heads of this group, Dr. R. Bhatnagar for initiation of Cu-HBrL activity and Sh. J. K. Mittal for further contribution to the program.

References

1. C. E. Little ed., Metal Vapour Lasers (Wiley- 1999)
2. R. P. Mildren et. al., J. Phys. D: Appl. Phys. 31, 1812-1816 (1998)
3. N. V. Sabotinov et. al., IEEE J. Quant. Electron. 31(4), 747-753(1995)
4. D. R. Jones et. al., IEEE J. Quant. Electron. 30(10), 2385-2390 (1994)
5. R. Biswal et. al., Pramana - Journal of Physics (Springer) 75(5), 953-959 (2010)
6. P. Countance et. al., IEEE J. Quant. Electron. 34(8), 1340-1346 (1998)
7. F. Girard et. al., J. Appl. Phys. 89(2), 843-848, (2001)
8. R. Biswal et. al., in Laser and Bose Einstein Condensation Physics; Manmohan et. al. Eds., 149-160 (Narosa: 2010)
9. R. Biswal et. al., Proc. of DAE-BRNS National Laser Symp. (NLS-20), Anna Univ., Chennai, 16-19 (2012)
10. P. K. Agrawal et. al., Proc. of DAE-BRNS National Laser Symp. (NLS-3), IIT, Kharagpur, 22-24 (2003)
11. P. K. Agrawal et. al., Proc. of DAE-BRNS National Laser Symp.(NLS-9), BARC, Mumbai , art. No.: CP-01-06 (2010)
12. R. Biswal et. al., Journal of Russian Laser Research (Springer), 33(4),319-335 (2012)
13. R. Biswal et. al., Optical Engineering 51(11), art No.114203, 1-8 (2012)
14. R. Biswal et. al., Optical Engineering 50(8), art. No. 084202, 1-8 (2011)
15. R. Biswal et. al., Proc. of DAE-BRNS National Laser Symp. (NLS-6), RRCAT, Indore, 43-44 (2006)
16. A. A. Isaev et. al., IEEE J. Quant. Electron. QE-33(6), 919-926 (1998)
17. R. Biswal et. al., IEEE J. Quant. Electron. 50(2), 112-119 (2014)
18. S. K. Dixit et. al., Optics Comm. 281, 2590-97 (2008)
19. R. Biswal et. al., Applied Optics 52(14), 3269- 3278 (2013)
20. G. K.Mishra et. al., Optik - Int. J. of Light Electron Optics 124, 1595-1600 (2013)